

Signal Transduction:
**Pancreatic Polypeptide is Recognized by
Two Hydrophobic Domains of the Human
Y4 Receptor Binding Pocket**

SIGNAL TRANSDUCTION



Xavier Pedragosa-Badia, Gregory R. Sliwoski,
Elizabeth Dong Nguyen, Diana Lindner, Jan
Stichel, Kristian W. Kaufmann, Jens Meiler
and Annette G. Beck-Sickinger
J. Biol. Chem. published online December 27, 2013

Access the most updated version of this article at doi: [10.1074/jbc.M113.502021](https://doi.org/10.1074/jbc.M113.502021)

Find articles, minireviews, Reflections and Classics on similar topics on the [JBC Affinity Sites](http://www.jbc.org/).

Alerts:

- [When this article is cited](#)
- [When a correction for this article is posted](#)

[Click here](#) to choose from all of JBC's e-mail alerts

Supplemental material:

<http://www.jbc.org/content/suppl/2013/12/27/M113.502021.DC1.html>

This article cites 0 references, 0 of which can be accessed free at

<http://www.jbc.org/content/early/2013/12/27/jbc.M113.502021.full.html#ref-list-1>

Pancreatic polypeptide is recognized by two hydrophobic domains of the human Y₄ receptor binding pocket^{*s}

Xavier Pedragosa-Badia[†], Gregory R. Sliwoski[§], Elizabeth Dong Nguyen[§], Diana Lindner^{†1}, Jan Stichel[†], Kristian W. Kaufmann[§], Jens Meiler^{§2} and Annette G. Beck-Sickinger^{†2}

[†]From the Institute of Biochemistry, Faculty of Biosciences, Pharmacy and Psychology. Universität Leipzig, Leipzig, Germany and the [§]Center for Structural Biology, Vanderbilt University Medical Center, Nashville, TN, USA.

Running title: *An iterative study to identify the Y₄R binding pocket*

To whom the correspondence should be addressed:

Annette G. Beck-Sickinger, Institute of Biochemistry, Faculty of Biosciences, Pharmacy and Psychology, Universität Leipzig, Brüderstraße 34, 04103 Leipzig, Germany. Phone: +493419736900. Fax: +493419736909. E-mail: beck-sickinger@uni-leipzig.de

Jens Meiler, Center for Structural Biology, Vanderbilt University, 5144B Biosci/MRBIII, 465 21st Avenue South, Nashville, TN 37232-8725, USA. Phone: +16159365662. Fax: +16159362211. E-mail: jens@meilerlab.org

Keywords: G protein coupled receptors (GPCR), neuropeptide Y family, Y₄R, pancreatic polypeptide, mutagenesis, binding pocket, comparative models

Background: The Y₄R is involved in regulation of food intake and gastrointestinal transport

Results: Mutagenesis studies revealed five residues displaying a significant loss of potency for hPP

Conclusion: Top of TM1, TM6 and TM7 interact with the hY₄R native agonist hPP

Significance: Characterizing the structure of the Y₄R binding pocket is crucial for the development of new anti obesity drugs

ABSTRACT

Structural characterization of the human Y₄ receptor (hY₄R) interaction with human pancreatic polypeptide (hPP) is crucial, not only for understanding its biological function but also for testing treatment strategies for obesity that target this interaction. Here, the interaction of receptor mutants with pancreatic polypeptide analogs was studied through double cycle mutagenesis. To guide mutagenesis and interpret results, a 3-dimensional comparative model of the hY₄R-hPP complex was constructed based on all available class A G protein-coupled receptor (GPCR) crystal structures and refined using experimental data. Our study reveals that residues of the hPP and the hY₄R form a

complex network consisting of ionic interactions, hydrophobic interactions and hydrogen binding. Residues Tyr^{2.64}, Asp^{2.68}, Asn^{6.55}, Asn^{7.32} and Phe^{7.35} of Y₄R are found to be important in receptor activation by hPP. Specifically, Tyr^{2.64} interacts with Tyr²⁷ of hPP through hydrophobic contacts. Asn^{7.32} is affected by modifications on position Arg³³ of hPP, suggesting a hydrogen bond between these two residues. Likewise we find that Phe^{7.35} is affected by modifications of hPP in position 33 and 36, indicating hydrophobic interactions between these three amino acids. Taken together, we demonstrate that the top of transmembrane helix 2 (TM2) and the top of transmembrane helices 6 and 7 (TM6-TM7) form the core of the peptide binding pocket. These findings will contribute to the rational design of ligands that bind the receptor more effectively to produce an enhanced agonistic or antagonistic effect.

G protein-coupled receptors (GPCRs) are the most prominent group of cell surface proteins. They are formed by 7 transmembrane helices (TM) that are connected by intracellular and extracellular loops (ECL). GPCRs can be activated by several stimuli such as hormones, light, or odorant molecules (1). It is estimated that

approximately 30% of all prescribed pharmaceuticals modify the activity of GPCRs (2) indicating that these receptors are fundamental drug targets in modern pharmacology.

The Y₄ receptor (Y₄R) is a member of the neuropeptide Y receptor family (NPYR), a class A GPCR family composed of Y₁R, Y₂R, Y₄R and Y₅R receptors in humans. The NPYR is closely related to other class A GPCR families such as the neuropeptide FF receptor family (NPFFR) and the orexin receptor family (OxR) (3). NPY receptors are physiologically coupled to the G_i or G_o proteins, however other reports show that rabbit Y₂R and rabbit Y₄R are also coupled to the G_q protein, triggering an increase in inositol phosphate (4). These receptors are activated by the NPY family of peptide hormones, consisting of neuropeptide Y (NPY), peptide YY (PYY) and pancreatic polypeptide (PP). NPY peptides and receptors form a multiligand/multireceptor system that plays a role in several physiological and pathological processes such as obesity and cancer (5). NPY peptides consist of 36 amino acids, are C-terminally amidated, and share high sequence identity. Shared structural features include a C-terminal helix. Despite high sequence homology and common structural features among NPY receptors and peptide hormones, however, there are significant differences in the affinity of these peptide hormones to the different receptor subtypes as well as differences in how the peptides bind their receptor (6).

The Y₄R, cloned in 1995 (7), has 375 amino acids and was found to be expressed in the colon, small intestine, pancreas, prostate (8), brain, and coronary arteries (7). Physiologically, the Y₄R is involved in the regulation of food intake (9), colonic anion transport (10), and adipose tissue and bone formation synergistically with Y₂R (11). The Y₄R sequence is one of the least conserved members of the NPYR family among different species, making it the fastest evolving functional member of the family (12). This makes it difficult to transfer conclusions from other Y receptor members to this subtype. Its main agonist, hPP, is produced by endocrine cells of the Langerhans islets of the duodenal part of the pancreas. These cells are also found in the gastrointestinal tract (13), albeit in much lower numbers. hPP was the first member of the NPY family of peptides to be identified. It is secreted after food ingestion in proportion to its caloric content (14) and it

promotes appetite suppression and inhibition of gastric emptying (15). This ligand was already found in ancient tetrapod evolution and appears to be one of the fastest developing peptides of the family (12). Because of its role in appetite suppression, this system is a very attractive target for the design of new therapeutic compounds for fighting obesity.

Detailed knowledge of the receptor-peptide interaction is essential for rational structure-based drug design. Although several studies characterizing the binding pocket of NPY receptors have been published in the past years (6,16-19), little is known about the Y₄R. To our knowledge, only one study describes a subtype selective interaction between Y₄R and its ligand hPP (20) where the conserved residue Asp^{6.59} of human Y₁R/Y₄R binds to Arg³⁵ of the peptides pNPY or hPP. In contrast Asp^{6.59} of hY₂R and hY₅R interact via Arg³³ of pNPY and pPYY. The importance of this conserved residue was later identified in other systems closely related to the NPYR, such as the NPFF receptor 1 and 2 systems (3) or the prolactin-releasing peptide receptor (PrRPR) (21).

In the present study, we characterize in detail for the first time structural determinants of the hPP/hY₄R interaction. Residues located at extracellular regions of the hY₄R, chosen according to their location in the receptor sequence and in comparative models of hY₄R, were mutated to determine their role in hPP binding. Simultaneously, a set of hPP analogs was also developed to pin-point specific interactions between hPP and hY₄R. We identified Tyr^{2.64}, Asp^{2.68}, Asn^{6.55}, Asn^{7.32} and Phe^{7.35} as members of the hY₄R binding pocket. Furthermore, hPP analogs with modifications in residues 27, 33 or 36 revealed these positions to be interaction partners with the receptor. These results clearly demonstrate the importance of the top of transmembrane helix 2 (TM2) and the top of transmembrane helices 6 and 7 (TM6 and 7) for hPP binding and illustrate the complexity of the intermolecular interactions within the hY₄R subtype.

EXPERIMENTAL PROCEDURES

Peptide synthesis- Peptides were synthesized by automated solid-phase peptide synthesis (SPPS) on a Syro II peptide synthesizer (MultiSynTech, Bochum, Germany) and manual

coupling steps following a 9-fluorenylmethoxycarbonyl-*tert*-butyl (Fmoc/*t*Bu) strategy as previously described with minor modifications (3). All peptides were synthesized on Rink amide resin (15 μmol scale) in order to obtain C-terminally amidated peptides. Amino acid coupling steps were performed with equimolar amounts of *N,N'*-diisopropylcarbodiimide (DIC)/hydroxybenzotriazole (HOBt) or *N,N'*-diisopropylcarbodiimide (DIC)/ethylcyanoglyoxylat-2-oxime (Oxyma). The cleavage from the resin was carried out using a mixture of trifluoroacetic acid (TFA)/thioanisole/ethanedithiol (EDT) (90:7:3 v/v/v). After full cleavage, a reducing mixture containing TFA/EDT/trimethylsilylbromide (TMsBr) was applied to reduce oxidized methionine. Crude peptides were purified using preparative reversed-phase high-performance liquid chromatography (RP-HPLC) on a Phenomenex C18 Jupiter 10 μ column (Proteo, 250 x 21.20 mm, 90 Å).

Peptide characterization was achieved by matrix assisted laser desorption/ionization (Ultraflex III MALDI-ToF/ToF, Bruker Daltonics, Billerica, MA, USA) and by electrospray ionization mass spectrometry. Peptide purities were determined on two analytical RP-HPLC systems using a linear gradient of 0.1% (v/v) TFA in H₂O (eluent A) and 0.08% (v/v) TFA in acetonitrile (ACN) (eluent B). The gradient used was 20-70 % of eluent B in eluent A in 40 min. The purity of the synthetic peptides was higher than 92% (data not shown).

Preparation of hY₄R mutants- The single mutations were inserted by site-directed mutagenesis into the protein sequence. Pfu Turbo DNA polymerase (Agilent, USA) (2.5 U/μl) was used as a reaction enzyme in combination with 10x reaction buffer. The plasmid hY₄_EYFP_N1 was used as a template (50-100 ng) and sense/antisense oligonucleotides were used in 2.5-10 pmol/μl concentrations depending on the reaction conditions. The deoxyribonucleotides (dNTP) mix was added in 10 mM concentration and dimethyl sulfoxide (DMSO) was used occasionally to reduce secondary structures. Dpn I (Thermo Fischer Scientific, USA) was used to eliminate the original dsDNA template. Constructs were transformed in semi-competent *E. coli DH5α* or *E. coli JM109* cells and the plasmid DNA was isolated using a Wizard plus Mini or Midi DNA purification system kit (Promega, USA). The

desired mutations were confirmed by sequencing of the complete coding sequence. The mutated positions are named after the system of Ballesteros and Weinstein (22).

Cell culture- HEK293 cells (human embryonic kidney) and COS-7 cells (African green monkey) were cultured as described previously (21).

Fluorescence microscopy studies- HEK293 cells were seeded and transfected with cDNA encoding hY₄R constructs as earlier described (23). The nuclei was stained with Hoechst 33342 (0.5 mg/ml) for 10 min after starving the cells for 20 min in OPTI[®]-MEM medium. Fluorescence microscopy pictures were captured using an ApoTome Imaging system with an Axio Observer microscope (Carl Zeiss, Jena, Germany).

Signal transduction assays- Signal transduction assays were performed on 24 or 48 well plates as previously described with minor changes (3,23). As transfection reagents Metafectene and Metafectene Pro (Biontex) were used. The analysis of the data obtained was performed using the Graph Pad Prism 5.03 software (GraphPad Software, San Diego, CA, USA). For each hypothesis the data was processed using a non linear regression analysis, obtaining concentration response curves displaying EC₅₀ and E_{max} values. Furthermore, EC₅₀ ratios were calculated using the global curve fitting function from Graph Pad Prism 5.03. All the experiments were performed in duplicates of at least two independent experiments.

Fourteen experimental GPCR structures were considered as templates for hY₄R comparative modeling- A comparative model of hY₄R was constructed using the protein structure prediction software package Rosetta, version 3.4 (24). Fourteen experimental GPCR structures from the Protein Data Bank (PDB) were considered as possible templates. These structures include rhodopsin (PDB ID: 1U19) (25), β₂-adrenergic receptor (PDB ID: 2RH1) (26), β₁-adrenergic receptor (PDB ID: 2VT4) (27), A_{2A} adenosine receptor (PDB ID: 3EML) (28), CXC chemokine receptor type 4 (CXCR4, PDB ID: 3ODU) (29), D₃ dopamine receptor (PDB ID: 3PBL) (30), H₁ histamine receptor (PDB ID: 3RZE) (31), M₂ muscarinic receptor (PDB ID: 3UON) (32), sphingosine-1-phosphate receptor (PDB ID: 3V2W) (33), M₃ muscarinic receptor (PDB ID:

4DAJ) (34), κ opioid receptor (PDB ID: 4DJH) (35), μ opioid receptor (PDB ID: 4DKL) (36), nociceptin/orphanin FQ opioid receptor (PDB ID: 4EA3) (37), and δ opioid receptor (PDB ID: 4EJ4) (38).

These structures were aligned with MUSTANG (39) and the resulting multiple sequence alignment (MSA) was aligned with a MSA of hY₁R, hY₂R, hY₄R, and hY₅R using CLUSTALW (40). Sequence alignments were adjusted to remove gaps within trans-membrane α -helices and ensure that highly conserved residues remain aligned (Figure S1). hY₄R residues were threaded onto the three-dimensional coordinates of aligned residues in each of the 14 GPCRs.

Missing atom coordinates were constructed using Rosetta loop construction protocols - Missing density and loop regions were reconstructed using Monte Carlo Metropolis (MCM) fragment replacement and cyclic coordinate descent (CCD) loop closure algorithms in Rosetta (41). All models underwent repacking and gradient minimization with RosettaMembrane (42). An additional constraint was included to account for the expected disulfide bond between hY₄R residues Cys^{3,25} and Cys^{5,25}.

The final set of models was clustered based on RMSD using bcl::Cluster (43). The top scoring models from the five largest clusters were used for docking studies.

Docking of pancreatic polypeptide (PP) into the comparative model of hY₄R- A set of nuclear magnetic resonance (NMR) structure conformations of bovine pancreatic polypeptide (PDB ID: 1LJV) (44) was docked into the hY₄R comparative models. bPP differs only on positions 6 and 23 with respect to hPP and has similar affinity for the hY₄R as earlier reported (45,46). The use of 1LJV provided a guide for the structural distinction between the peptide's helical region and dynamic tail region. The helical region (residues 14-31 PEQMAQYAAELRRYINML) was first docked into the hY₄R models. Four distinct helix conformations were docked into 37 hY₄R comparative models without ECLs, guided by a predicted interaction between hY₄R Tyr^{2,64} and hPP Tyr²⁷.

C-terminal residues of hPP were added using de novo folding with experimental restraints- The five C-terminal residues of hPP (TRPRY) were constructed using Rosetta's low resolution *de novo* folding algorithm where

residues are represented as "centroids" (47). Three experimentally-derived restraints between hY₄R and PP residues were used to guide this step using an 8 Å distance cutoff between residues: Asp^{6,59} and Arg³⁵, Phe^{7,35} and Arg³³, and Asn^{7,32} and Arg³³ (20,48). All restraints are detailed in Table 1.

The ECLs were rebuilt as described for the comparative modeling of hY₄R, with the addition of these experimental constraints. Additionally, these models were refined to atomic detail, replacing centroids with side chain rotamers based on a backbone-dependent rotamer library and energy minimization with RosettaMembrane (49-51).

Models were relaxed using atomic-resolution experimental restraints- Models were again clustered based on RMSD. Top scoring models from the largest clusters were visually inspected for binding poses that preserved the experimental restraints. Selected models underwent an additional relaxation step with constraints adjusted to reflect atomic-level interactions between residues Asp^{6,59} and Arg³⁵ (three Å distance between the two δ -oxygen atoms on Asp^{6,59} and the side-chain nitrogen atoms on Arg³⁵), and residues Asn^{7,32} and Arg³³ (four Å distance between the δ -oxygen atom on Asn^{7,32} and the two side chain nitrogen atom on Arg³³). These constraint distances allow for possible hydrogen bonding and salt bridge interactions. An additional restraint between hY₄R Phe^{7,35} and PP Tyr³⁶ was introduced. Final models were clustered and visually inspected and 9 representative models were selected. The overall workflow for receptor modeling and peptide docking is summarized in Figure 1.

RESULTS

The comparative models presented here reflect an iterative process where multiple rounds of modeling were performed in parallel with *in vitro* experiments. Early models were generated based on comparative modeling with only seven GPCR templates and limited experimental restraints. The number of templates eventually increased to fourteen as more GPCR structures became available. Additionally, predicted interactions seen in earlier models were used to guide some of the mutational assays. These assays provided additional restraints that were included in later models. The final models represent one plausible way that binding between hPP and hY₄R

can occur based on all experimental evidence available.

Tyr^{2.64} of TM2 interacts with Tyr²⁷- Tyr^{2.64} is located on top of TM2 and was found to be important in hY₁R (16). This amino acid is conserved in all receptor subtypes except of hY₅R (Figure 2B), therefore we hypothesized that this amino acid would be relevant in hY₄R. To investigate Tyr^{2.64}, this position was mutated to Ala and showed a significant shift of the EC₅₀ value with 65-fold loss of potency but with 130% of efficacy (Figure 3A). This high efficacy value matches with excellent membrane localization of the receptors revealed by fluorescence microscopy studies. Furthermore, the modification of Tyr^{2.64} to the larger aliphatic amino acid, Leu, was much better tolerated and displayed wild type-like activity with slightly reduced efficacy (83%). Furthermore, to test the importance of the hydroxyl moiety at this position, the mutant Tyr^{2.64}Phe was constructed. The native ligand hPP displayed a 4-fold loss of potency and wild type like efficacy (94%).

Since Ala-scan studies of pNPY (52) revealed Tyr²⁷ as an important position for pNPY binding on hY₄R, this led to the hypothesis this residue might be the interaction partner of Tyr^{2.64}. To investigate the role of Tyr²⁷, the analogs [Ala²⁷]hPP, [Leu²⁷]hPP, [Cha²⁷]hPP and [Phe²⁷]hPP were synthesized. The substitution of Tyr²⁷ to Leu pursued the aim of introducing a longer aliphatic amino acid whereas the introduction of Cha was constructed to investigate the effects of a more bulky hydrophobic amino acid. Additionally, the substitution of Tyr²⁷ to Phe was made to investigate the relevance of the hydroxyl group and discarding a possible hydrogen bond. [Ala²⁷]hPP displayed an 8-fold loss of activity (EC₅₀ 11.78 nM), whereas the Leu, Cha variants showed wild type like potency on hY₄R (Table 2). To investigate the effect of modifications on position Tyr²⁷ with a hypothetical interaction to Tyr^{2.64}, the mutants Tyr^{2.64}Ala and Tyr^{2.64}Leu were also tested with the peptide analogs in a double-cycle mutagenesis approach. [Ala²⁷]hPP revealed a dramatic activity shift when tested on Tyr^{2.64}Ala (424-fold), whereas [Leu²⁷]hPP displayed no further loss on Tyr^{2.64}Ala (Figure 3A). In contrast, [Cha²⁷]hPP activated Tyr^{2.64}Ala with higher potency (EC₅₀ 22.34 nM) compared to hPP. However, testing [Ala²⁷]hPP on Tyr^{2.64}Leu displayed a great activity loss of 138-

fold (EC₅₀ 205.20 nM), while [Leu²⁷]hPP and [Cha²⁷]hPP activated Tyr^{2.64}Leu with a moderate loss of potency of 21 to 23-fold compared to hY₄R with hPP (Table 2). Besides these findings, [Phe²⁷]hPP was tested with Tyr^{2.64}Phe to further investigate the interaction type. [Phe²⁷]hPP displayed only a 9-fold loss of potency on Tyr^{2.64}Phe. Taken together, this confirms that the presence of a bulky hydrophobic amino acid is favorable for this interaction site of the binding pocket and suggests that Tyr^{2.64} might interact with a second amino acid. This is supported by the comparative models, since seven models have Tyr^{2.64} within 8 Å of Tyr²⁷ and eight models have Tyr^{2.64} within 8 Å of Leu³¹, which might be the second interaction point. Nevertheless, experimental data is needed to confirm this second interaction point.

Other positions highlight the importance of ECL1- Another amino acid investigated was Asp^{2.68}. This residue is conserved in all receptor subtypes except in hY₂R (Figure 2B), which contains Gly at this position. Asp^{2.68} was found to be important in mutagenesis studies on the hY₁R (17) and it is one of the interaction points between receptor and NPY on the hY₅R system (6). In hY₄R the exchange of Asp^{2.68} to Ala led to a 94-fold loss in activity and decreased the efficacy dramatically to 39% of the wild-type receptor response (Figure 3B, Table 3). The loss in efficacy fits with the high intracellular accumulation of receptors demonstrated by fluorescence microscopy (Figure 4). In contrast, the exchange to Glu or Asn regained the efficacy (93 to 87% respectively) and displayed a loss of potency for hPP only 9 and 16-fold, respectively.

Additionally, position Trp^{2.70}, which is conserved in all receptor subtypes, was described in some GPCR to belong to the motif WXFG and to be important for receptor activation (53). To prove its relevance, Trp was mutated to Ala, leading to a 107-fold loss in potency. Mutation to Tyr displayed only a 2-fold loss of potency (Table 3). These exchanges reveal that an aromatic or bulky side chain is necessary in this position to keep wild type-like activity.

The tested residues in TM3, ECL2 and TM5 do not play a relevant role in the binding pocket- The single residue tested in TM3 was Gln^{3.32}. This position has been shown to participate in the binding pocket of nearly all crystallized class A GPCRs (2). In the hY₄R, the exchange to

Ala of Gln^{3.32} displayed a wild type-like potency when tested with hPP.

The ECL2 is the least conserved region between receptor subtypes. To elucidate the role of this ECL, several amino acids were mutated to Ala (Figure 2C). In order to investigate polar interactions with the positively charged residues of the peptide Arg³³ and Arg³⁵, amino acids with negatively charged side chains Glu^{4.67}, Glu^{4.79}, and Asp^{4.83} were mutated to Ala. These three Ala mutants revealed wild type-like activity with EC₅₀ values from 1 to 2 fold over hY₄R. Furthermore, preliminary comparative models suggested that the residues Lys^{4.72}, Phe^{4.80}, Trp^{5.29}, His^{5.34}, Tyr^{5.38} and Phe^{5.41} located on ECL2 and top of TM5 might be involved in the receptor binding pocket. The exchange of Lys^{4.72}, Trp^{5.29} and Phe^{5.41} to Ala displayed only a 3 to 4-fold loss of potency when tested with hPP. Phe^{4.80} and His^{5.34} revealed wild type-like potency for hPP when exchanged to Ala. Only Tyr^{5.38} showed a reduced efficacy for hPP (43%, Table 4) but wild type like potency. A further mutation to Ser in this position led to a partial regain of efficacy and displayed 3-fold loss of potency for hPP, whereas an additional exchange to Phe of this position, to proof the relevance of the hydroxyl moiety, led to wild type like potency for hPP.

TM6 plays a crucial role in building the binding pocket - Asp^{6.59} on top of TM6 has already been shown to form a direct contact to the ligand (20). To further characterize the role of this part of the receptor, residues in close proximity to Asp^{6.59} were chosen for further mutagenesis studies. Phe^{6.54} was mutated to Ala because of its importance in other GPCRs closely related to the hY₄R, its aromatic character and its close proximity to Asp^{6.59}. Phe^{6.54}Ala displayed a 4-fold loss of hPP potency with reduced efficacy (73%, Table 4) that corresponds with poor membrane localization observed by fluorescence microscopy (Figure 4). Asn^{6.55} was found to be involved in the hY₁R binding pocket (18) and because initial comparative models oriented the side chain of this amino acid towards the interior of the hY₄R binding pocket, this indicated its possible involvement in ligand receptor interactions. Stimulation of Asn^{6.55}Ala with hPP resulted in an 8-fold loss in activity and 79% of efficacy (Figure 5A, Table 5) suggesting that this position is important in the receptor pocket.

Additionally, His^{6.62} was investigated because of its proximity to Asp^{6.59} at the beginning of ECL3. His^{6.62}Ala revealed an EC₅₀ of 0.4 nM, which is moderately better than wild type.

TM7 is a contact point of hPP in the hY₄R, Asn^{7.32} interacts with Arg³³ of hPP.- The first position investigated in TM7 was Asn^{7.32}. This residue was found to be relevant for PYY binding on the Y₁R (54) and initial comparative models indicated the possible importance of this position as well. Asn^{7.32} was mutated to Ala, Arg and Asp. The effect of these substitutions increased in the following manner: Arg>Ala>Asp (Table 5, Figure 5B). This suggested that the introduction of a positive charge might cause a repulsion that was eliminated with the introduction of the negative charge Asp. Hence, we supposed that one of the C-terminally positively charged Arg might be the interaction partner. Since Arg³⁵ of hPP was already identified to interact with hY₄R Asp^{6.59}, Arg³³ was suggested as a possible interaction partner of Asn^{7.32}. To clarify the binding hypothesis, the hPP analogs [ADMA³³]hPP, [SDMA³³]hPP and [Lys³³]hPP were synthesized. Position 33 of hPP was modified to symmetrically dimethylated Arg (SDMA) and asymmetrically dimethylated Arg (ADMA) to maintain the positive charge and simultaneously reduce the possibility of hydrogen bond formation. Whereas [Lys³³]hPP revealed wild type-like activity, the exchange of Arg to ADMA or SDMA displayed a 7-fold to 6-fold loss of activity (Table 5). Next, the hPP variants were tested on the receptor mutants Asn^{7.32}Ala and Asn^{7.32}Asp. [Lys³³]hPP displayed a great loss of activity on Asn^{7.32}Ala (60-fold, EC₅₀ 87.78 nM), [ADMA³³]hPP and [SDMA³³]hPP displayed a dramatic activity loss compared to the wild type peptide with EC₅₀ values 1416 nM and >2000 nM respectively (Table 5, figure 5B). These experiments demonstrated that the introduction of a shorter amino acid such as Lys was better tolerated than the double methylation of Arg, which was not tolerated at all. Unlike Asn^{7.32}Ala, Asn^{7.32}Asp showed only a 2 to 3-fold loss of potency when tested with [Lys³³]hPP and [ADMA³³]hPP, revealing that the introduction of the double methylation or the reduction of the side chain length did not affect the binding pocket.

Phe^{7.35} interacts with Arg³³ as well as Tyr³⁶.- Phe^{7.35} on the top of TM7 was also investigated, since this conserved position might be a suitable interaction point because of its

aromatic characteristics and location. Furthermore, in the hY₅R, Tyr^{7.35} was found to be relevant for the receptor and was suggested to belong to the receptor binding pocket (6). The initial comparative models also suggested its orientation to the interior of the proposed binding pocket. The amino acid was mutated to Ala and Ile, displaying a moderate loss in potency (7-fold) for the Ala mutant, whereas the Ile mutant revealed 41-fold loss of potency compared to wild type (Table 6). The higher potency loss caused by the Ile variant might indicate that the distance or the space available between Phe^{7.35} and the ligand or other positions in the receptor is important. Phe^{7.35}Ile also showed reduced efficacy that corresponds to high intracellular receptor localization as demonstrated by fluorescence microscopy (Figure 4). Preliminary comparative hY₄R models suggested that this residue was in close proximity to Arg³³ and Tyr³⁶. Furthermore, Arg³³ and Tyr³⁶ revealed to be critical residues for pNPY binding on the hY₄R (52). Taken all these facts together, we hypothesized that Phe^{7.35} might interact with one or both amino acids, Arg³³ or Tyr³⁶, of the peptide. As described above, the exchange of Phe^{7.35} to Ile displayed higher impact on receptor activity than the Ala substitution (Table 6). [Lys³³]hPP and [ADMA³³]hPP were used to investigate the relationship between Phe^{7.35} and Arg³³. [Lys³³]hPP displayed a dramatic loss of 451-fold in activation (EC₅₀ 640.4 nM) on Phe^{7.35}Ala. Following tests with [ADMA³³]hPP revealed a 107-fold loss of activity compared to hPP on Phe^{7.35}Ala. This corresponds to the potency loss produced by the mutant plus the loss produced by the analog. Lastly, Phe^{7.35}Ile leads to a dramatic loss in activity when tested with both analogs.

Preliminary models suggested Tyr³⁶ as a second interaction partner to Phe^{7.35}. In order to characterize this hypothetical interaction, several analogs with modifications on Tyr³⁶ were synthesized (Table 6). The introduction of Phe³⁶ was well tolerated on the hY₄R, indicating that the hydroxyl group of the side chain of Tyr was not playing a relevant role. The introduction of a non-aromatic amino acid such Ile brought a dramatic loss in potency on the wild type receptor (123-fold). Shortening the length of the side chain to Ala led to an even higher loss in potency (>2000-fold). Surprisingly, the introduction of unnatural amino acids such as Cha and Nle was better tolerated (EC₅₀ values 0.6 nM and 14.40 nM

respectively, Table 6, Figure 6). These hPP analogs were tested on Phe^{7.35}Ala to investigate the type of interaction between these two positions. Phe^{7.35}Ala showed a 17-fold loss of activity when tested with [Phe³⁶]hPP (EC₅₀ 25.29 nM). [Ile³⁶]hPP was not tolerated at all with Phe^{7.35}Ala. This peptide displayed a dramatic loss of activity (EC₅₀ N.D.), whereas Nle was slightly better tolerated revealing an EC₅₀ value 679-fold over wild type. Lastly, the second unnatural amino acid, [Cha³⁶]hPP, displayed a 138-fold loss of activity over wild type (EC₅₀ of 211.2 nM) on Phe^{7.35}Ala, and was thereby substantially better tolerated than Ile and Nle. Taken together, this indicates the need for a bulky hydrophobic amino acid in this position (Table 6, Figure 6).

The final comparative models support this results since within the nine best models obtained, 8 out of 9 showed Asn^{7.32} within 8 Å of distance to Arg³³ and 9 out of 9 models showed Phe^{7.35} within 8 Å of proximity to Arg³³ (Figure 8).

In addition to the residues mentioned above, the conserved residue His^{7.39} which was one helix turn deeper in TM7 was also investigated. The Ala mutant did not reveal any detectable activity and fluorescence microscopy pictures confirmed intracellular localization of the receptor. No further studies have been performed as this receptor variant is stuck in trafficking.

Docking of PP to the hY₄R comparative model- Pancreatic polypeptide was docked into the comparative model of hY₄R to assist interpretation of experimental results. Since inactive GPCR structures were used for our templates, it was important to consider the effects this may have on docking an agonist to this model.

Rosetta's comparative modeling protocol is insensitive to the state of GPCR templates. Templates are used only in the initial transmembrane helix positioning. Several relaxation steps allow for energy-based adjustments to these placements. Additionally, all extracellular loops are rebuilt in accordance with Rosetta's de novo folding algorithm. It is conceivable, however, that the helical conformations of an active template may be altered enough to fall outside of the conformational explored with inactive templates. We compared the RMSD of our templates with the latest agonist-bound GPCR crystal structures. Pair-wise alignments using the structure-based alignment tool MAMMOTH revealed that the

average RMSD of our inactive structures (2.9±.6) is not significantly different from that of the active structures (2.8±.6). Importantly, the average RMSD is unchanged when combining the two groups (3.1±.5).

In addition to our analysis, Tautermann and Pautsch examined the binding sites of active and inactive β₂-adrenergic receptor. They show that the binding site is very similar between the inactive and active states. Previous modeling studies with the inactive structure predicted the binding mode of an agonist that overlapped well with that seen in the agonist-bound crystal structure (55).

The initial placement of the PP helix was guided specifically by the altered activity of hY₄R Tyr^{2.64} and hPP Tyr²⁷ mutants (Table 2). This placement provided a starting position from which the dynamic ECLs and C-terminal tail of hPP might be folded to simulate additional interactions suggested by the mutational data. These interactions specifically include a predicted salt bridge between hY₄R Asp^{6.59} and PP Arg³⁵, a predicted hydrogen bond between hY₄R Asn^{7.32} and PP Arg³³, a predicted cation-π interaction between hY₄R Phe^{7.35} and PP Arg³³, and an interaction between hY₄R Phe^{7.35} and PP Tyr³⁶.

The restraints imposed by these experimental results were included initially as low resolution restraints based on residue proximity. To complete the model, several restraints were adjusted to higher resolution atom-level restraints in an attempt to capture the proposed interactions on an atomic level. The specific restraints imposed and their corresponding steps are described in Table 1. When PP was docked using the low resolution restraints, 81% of the generated models did not significantly violate any of the restraints. In the final step, when the high resolution restraints were imposed, 29.8% of the models generated were able to fit these restraints with no significant violations. This was encouraging in that a significant portion of our models were capable of fitting proposed atom-level interactions. A subset of nine top scoring models that showed no significant violation of high-resolution restraints was selected as the final ensemble for discussion. These models fit well with the majority of the experimental results, accurately portraying residues found to affect activity as well as those residues that failed to show any effect on activity. Specifically, the predicted salt bridge between

Asp^{6.59} and Arg³⁵ is well represented in eight of the nine models. All models show less than a 4.0 Å distance between both inter-residue oxygen-nitrogen pairs, providing possible salt bridge interactions or hydrogen bonding. Six of the nine models demonstrate a distance of less than 3.2 Å between the oxygen in hY₄R Asn^{7.32} and amine group in PP Arg³³, providing for the possibility of a hydrogen bond between these residues. hY₄R Phe^{7.35} and PP Arg³³ point towards each other in all nine models which is conducive to the proposed cation-π interaction. Additionally, hY₄R Phe^{7.35} and hPP Tyr³⁶ were orientated towards each other in four models. Finally, hY₄R Asp^{2.68} is within 8 Å and points towards the PP helix in five models, suggesting an interaction between the hPP helix and hY₄R Asp^{2.68}. One of the nine models is shown in figure 7A and 7B, highlighting the binding site and residues important for PP- hY₄R binding.

The importance of hY₄R Trp^{2.70} for hPP binding is the only experimental finding not well reflected in the models. In all but one of the nine models, it is pointing away and/or not in close proximity to hPP. Possible explanations include inaccuracy of the model in this region, increased dynamics of this region as displayed in our models, or an indirect effect that involves a second site on the receptor that interacts with both hPP and Trp^{2.70}. It is interesting that the length of TM2 varies in the models, thereby changing the length of the first intracellular loop dramatically from 3 residues in two of the models, 9-11 residues in five models, and 12-13 residues in two models. Since the models did not converge on a consistent length of ECL1, and precision is a prerequisite for accuracy, we expect that accuracy in this region might be low. This discrepancy in loop length is shown in Figure 7C.

The residues that failed to show a significant effect on activity in the mutational assays are generally not contacting PP in the model. The majority of these residues are located in ECL2 which is consistently localized on the edge of the receptor away from hPP. Specifically, Lys^{4.72}, Glu^{4.79}, Phe^{4.80}, Asp^{4.83}, His^{5.34}, and Phe^{6.54} are further than 8 Å away from any PP residue. Gln^{3.32}, Glu^{4.67}, Trp^{5.29}, His^{6.62}, and His^{7.39} are within 8 Å of a hPP residue in only three of the nine models, and Tyr^{5.38} is within 8 Å of a hPP residue in only two of the nine models. ECL2 and

the residues not involved in PP binding are shown in Figure 7D.

The ensemble of nine models was analyzed for ligand-receptor interactions. These predictions can serve as hypotheses to direct future mutational assays. Residue pairs between PP and hY₄R with a distance of less than 8 Å were collected across all nine models. The total counts are shown in Figure 8. This map can serve as a foundation from which to identify the residues that line the binding pocket. For example, five of nine models show that hY₄R Ser^{5,28} and PP Thr³² are within 8 Å of each other, suggesting a possible interaction between these two residues.

DISCUSSION

In the NPY receptor family, the ECL1 and TM6 were regions described to form the binding pocket and interact with the peptide (6,20). Additionally, hY₁R which shares high sequence homology with hY₄R, has been extensively characterized in the past. Many amino acids located on ECL1, TM6 and TM7 are crucial for the interaction (16,19,54). Taking all these data into consideration, we expected the hY₄R binding pocket to be composed of amino acids located in these areas of the receptor. Furthermore, it was also expected that hY₄R has a second interaction site with the peptide on top of TM2 or beginning of ECL1, as suggested for hY₅R (6).

We have now identified a hydrophobic binding pocket for the hY₄R system that is composed of several residues located on TM2, TM6 and TM7. The first identified position in the pocket, Tyr^{2,64}, is conserved in hY₁R, hY₂R and hY₄R. It is also present in the prolactin-releasing peptide receptor (PrRPR) from several species including human, rat, and mouse. Tyr^{2,64} was found to be involved in ligand binding on the hY₁R and was suggested to belong to a hydrophobic pocket (19). In the hY₄R, Tyr^{2,64} demonstrated that bulkiness and not aromaticity is critical for the interaction with hPP.

Tyr^{2,64}Leu displayed a small decrease in efficacy for hPP. This might be caused by a small portion of receptors being trapped intracellular (Figure 4). The substantial amount of intracellular accumulation could be due to high expression levels of the mutant receptor, albeit it is not very likely since all constructs share the same promoter. It is more probable that this intracellular increase is due to an impaired folding of the mutant.

However, the signal intensities suggest that enough active receptors are present in the cell membrane.

To elucidate a candidate position on the peptide side to interact with position Tyr^{2,64} of hY₄R, earlier Ala-scanning mutagenesis studies on the NPY peptide family were considered (56). Among others, Tyr²⁷ of NPY and PYY is relevant for binding in all NPY receptor subtypes (52,56). This conserved residue in the three peptide ligands of the NPY family was thought to be a likely candidate to interact with Tyr^{2,64} of hY₄R. Since Leu and Cha at position 27 of hPP have a non-planar configuration compared to the wild type Tyr, in presence of Leu or Cha on position 2,64 of hY₄R the interaction might be slightly impeded, and a lack of space between Tyr^{2,64} and Tyr²⁷ seems to be a limiting factor for the interaction to take place. This fact would support the close distance between these two positions suggested by the comparative models (Figure 7A). Additionally, a hydrogen bonding interaction could be discarded between hY₄R Tyr^{2,64} and hPP Tyr²⁷. Besides this, we could not explain the relevance of the hydroxyl moiety of Tyr^{2,64} since an aromatic amino acid lacking the hydroxyl moiety like Phe is not as well tolerated as a hydrophobic amino acid like Leu. One hypothesis could be that Phe would adopt a slightly different orientation than Tyr or Leu and therefore the interaction with the ligand could be slightly impeded. Overall, our data is most consistent with a hydrophobic interaction between hY₄R Tyr^{2,64} and hPP Tyr²⁷. Furthermore, the fact that the activity shift obtained for Tyr^{2,64}Ala with hPP was larger than the shift obtained for [Ala²⁷]hPP on hY₄R would indicate that Tyr^{2,64} might interact with another position in the peptide or within the receptor.

Confirming the importance of ECL1, the nearby residues Asp^{2,68} and Trp^{2,70} proved critical for the hY₄R/hPP interaction. Asp^{2,68}Ala displayed high loss of potency and efficacy for hPP. Further mutations on Asp^{2,68} suggest that perhaps a polar or negatively charged amino acid is needed for correct export to or stability in the membrane. The relevance of this position is supported by the fact that on the hY₅R Asp^{2,68} has been proven to interact with Arg²⁵ of pNPY (6). Additionally this residue was hypothesized to form electrostatic interactions with NPY in the hY₁R (17,19). On hY₄R, Asp^{2,68} may form hydrogen bonds with the peptide. Also, a polar effect on the structure which

stabilizes the receptor binding pocket might be a feasible function for this position. The nearby residue Trp^{2.70} needs a bulky hydrophobic amino acid. Although the models show this residue not directly pointing to the peptide, further data are needed to elucidate the role of this residue on the hY₄R binding pocket. This position could participate on direct ligand binding or have a more structural role affecting the nearby important positions when mutated.

On TM6, Asn^{6.55} participates in the binding pocket of the hY₄R. Our results are supported by the loss in NPY binding displayed by Asn^{6.55}Ala on studies with the hY₁R (18). The comparative models demonstrate this amino acid pointing to the inner side of the proposed binding pocket close to Phe^{7.35} (Figure 7A-B). Asn^{6.55} is a candidate for interaction with Arg³³ of hPP as in six models these residues are within a distance of 8 Å (Figure 8). Moreover as recently reported, this position is involved in ligand receptor interactions of many crystallized class A GPCRs (2). This fact strongly supports our data and confirms the role that Asn^{6.55} of hY₄R has in the hPP binding pocket.

The results obtained on position Asn^{7.32} suggest that this residue is a key player in the binding pocket of hY₄R. The mutation to Ala displays a small loss in potency for hPP. On prior studies on the hY₁R, PYY and 1229U91 (GR231118), a Y₄R agonist, and a Y₁R antagonist, displayed a loss in binding for Asn^{7.32}Ala (54). It could be shown that Asn^{7.32} might be in close proximity with a positively charged residue, probably one of the two Arg of the C-terminal segment of hPP. To characterize the relationship between hY₄R Asn^{7.32} and Arg³³ of hPP, position 33 was modified to Lys to investigate the influence of the side chain length. Also asymmetric and symmetric side chain dimethylations were tested at this position. Side chain methylations block hydrogen-bond donor positions and increase hydrophobicity and bulkiness of the residue (57). Furthermore, the ability to form polar interactions such as dipole-dipole interactions might be impeded by double side chain methylation. The asymmetric and symmetric double methylation on position Arg³³ of hPP produced a potency loss (6 to 7-fold) on hY₄R, probably by blocking potential hydrogen bonding positions, potential dipoles or due to steric hindrance. On Asn^{7.32}Ala, the double side chain methylation of position Arg³³ of hPP had a

more dramatic effect. This might cause conformational changes in doubly methylated Arg³³ of hPP impeding interactions with close by residues such as Phe^{7.35}. These data are in agreement with the shortening of the side chain in [Lys³³]hPP that resulted in a smaller potency loss on Asn^{7.32}Ala, suggesting that Asn^{7.32} and Arg³³ of hPP are in very close proximity. The fact that these three peptide analogs displayed potencies similar to wild type on Asn^{7.32}Asp also supports an interaction with Arg³³, since Asp maintains the hydrogen bonding capability and incorporates a negative charge able to form an ionic bond with position Arg³³. Accordingly, we were able to demonstrate that Asn^{7.32} interacts with Arg³³ possibly by hydrogen bonding or polar interactions. This hypothesis is supported by the great relevance of Arg³³ as already demonstrated in the Ala-scan (52). Comparative models where Arg³³ of hPP is located between Asn^{7.32} and Phe^{7.35} of hY₄R nicely reflect this hypothesis. (Figure 7B).

The last residue of the proposed hydrophobic binding pocket is Phe^{7.35}. The exchange of Phe^{7.35} to Ile led to a higher potency and efficacy loss than the exchange to Ala, possibly due to steric hindrance. This position has been found to belong to the binding pocket of several class A GPCRs, among them the peptide receptors hCXCR4 and the rat neurotensin receptor 1 (NTSR1) (2). Furthermore, this position might highlight the singularity of the Y₄R binding pocket with respect to the Y₁R. To investigate the role of hydrophobicity and size of Arg³³ of hPP towards Phe^{7.35} of hY₄R, [ADMA³³]hPP was tested on Phe^{7.35}Ala. The obtained results fit with the higher potency of [ADMA³³]hPP compared to [Lys³³]hPP on Phe^{7.35}Ala, because the methyl groups can reduce the distance between both positions. A second interaction point of Phe^{7.35} was suggested by preliminary models to be Tyr³⁶ as hypothesized in previous studies on the Y₁R (58). The fact that an aliphatic amino acid such as Ile with a branched β-carbon is not tolerated in contrast to Cha or Phe, could suggest a need for space close to the peptide backbone. On the other hand, the effect of these ligands on Phe^{7.35}Ala indicates that in absence of Phe in position 7.35, an aromatic amino acid must be present on position 36 of hPP. This may arise for conformational reasons as only an aromatic amino acid with a planar structure might be able to contact position 7.35 in the absence of Phe. So, in

the presence of both aromatic groups a π - π interaction might be established between Phe^{7,35} and Tyr³⁶. In the absence of the aromatic group on position 36 of hPP, this residue might form hydrophobic interactions instead.

Our data provide the first insights into the complex binding pocket of the hY₄R-system derived from a combination of modeling and mutagenesis. As it may not be possible to solve the structure of all GPCRs, we demonstrate that this iterative method of study is very promising for understanding structurally uncharacterized receptors. As the model is in agreement with experimental data, it can be used to generate further testable hypotheses regarding the receptor-peptide interaction contributing to the development of ligands with enhanced hY₄R activity.

REFERENCES

1. Zhang, R., and Xie, X. (2012) Tools for GPCR drug discovery. *Acta Pharmacol. Sin.* **33**, 372-384
2. Venkatakrishnan, A. J., Deupi, X., Lebon, G., Tate, C. G., Schertler, G. F., and Babu, M. M. (2013) Molecular signatures of G-protein-coupled receptors. *Nature* **494**, 185-194
3. Findeisen, M., Rathmann, D., and Beck-Sickinger, A. G. (2011) Structure-activity studies of RFamide peptides reveal subtype-selective activation of neuropeptide FF1 and FF2 receptors. *ChemMedChem* **6**, 1081-1093
4. Misra, S., Murthy, K. S., Zhou, H., and Grider, J. R. (2004) Coexpression of Y1, Y2, and Y4 receptors in smooth muscle coupled to distinct signaling pathways. *J. Pharmacol. Exp. Ther.* **311**, 1154-1162
5. Pedragosa Badia, X., Stichel, J., and Beck-Sickinger, A. G. (2013) Neuropeptide Y receptors: How to get subtype selectivity. *Front. Endocrinol. (Lausanne)* **10**.3389/fendo.2013.00005
6. Lindner, D., van Dieck, J., Merten, N., Morl, K., Gunther, R., Hofmann, H. J., and Beck-Sickinger, A. G. (2008) GPC receptors and not ligands decide the binding mode in neuropeptide Y multireceptor/multiligand system. *Biochemistry* **47**, 5905-5914
7. Bard, J. A., Walker, M. W., Brancheck, T. A., and Weinshank, R. L. (1995) Cloning and functional expression of a human Y4 subtype receptor for pancreatic polypeptide, neuropeptide Y, and peptide YY. *J. Biol. Chem.* **270**, 26762-26765
8. Lundell, I., Blomqvist, A. G., Berglund, M. M., Schober, D. A., Johnson, D., Statnick, M. A., Gadski, R. A., Gehlert, D. R., and Larhammar, D. (1995) Cloning of a human receptor of the NPY receptor family with high affinity for pancreatic polypeptide and peptide YY. *J. Biol. Chem.* **270**, 29123-29128
9. Li, J. B., Asakawa, A., Terashi, M., Cheng, K., Chaolu, H., Zoshiki, T., Ushikai, M., Sheriff, S., Balasubramaniam, A., and Inui, A. (2010) Regulatory effects of Y4 receptor agonist (BVD-74D) on food intake. *Peptides* **31**, 1706-1710
10. Tough, I. R., Holliday, N. D., and Cox, H. M. (2006) Y(4) receptors mediate the inhibitory responses of pancreatic polypeptide in human and mouse colon mucosa. *J. Pharmacol. Exp. Ther.* **319**, 20-30
11. Sainsbury, A., Baldock, P. A., Schwarzer, C., Ueno, N., Enriquez, R. F., Couzens, M., Inui, A., Herzog, H., and Gardiner, E. M. (2003) Synergistic effects of Y2 and Y4 receptors on adiposity and bone mass revealed in double knockout mice. *Mol. Cell. Biol.* **23**, 5225-5233
12. Wraith, A., Tornsten, A., Chardon, P., Harbitz, I., Chowdhary, B. P., Andersson, L., Lundin, L. G., and Larhammar, D. (2000) Evolution of the neuropeptide Y receptor family: gene and chromosome duplications deduced from the cloning and mapping of the five receptor subtype genes in pig. *Genome Res.* **10**, 302-310
13. Ekblad, E., and Sundler, F. (2002) Distribution of pancreatic polypeptide and peptide YY. *Peptides* **23**, 251-261
14. Perry, B., and Wang, Y. (2012) Appetite regulation and weight control: the role of gut hormones. *Nutr. Diabetes* **2**, e26
15. Zhang, L., Bijker, M. S., and Herzog, H. (2011) The neuropeptide Y system: pathophysiological and therapeutic implications in obesity and cancer. *Pharmacol. Ther.* **131**, 91-113
16. Sautel, M., Martinez, R., Munoz, M., Peitsch, M. C., Beck-Sickinger, A. G., and Walker, P. (1995) Role of a hydrophobic pocket of the human Y1 neuropeptide Y receptor in ligand binding. *Mol. Cell. Endocrinol.* **112**, 215-222
17. Walker, P., Munoz, M., Martinez, R., and Peitsch, M. C. (1994) Acidic residues in extracellular loops of the human Y1 neuropeptide Y receptor are essential for ligand binding. *J. Biol. Chem.* **269**, 2863-2869
18. Sautel, M., Rudolf, K., Wittneben, H., Herzog, H., Martinez, R., Munoz, M., Eberlein, W., Engel, W., Walker, P., and Beck-Sickinger, A. G. (1996) Neuropeptide Y and the nonpeptide antagonist BIBP 3226 share an overlapping binding site at the human Y1 receptor. *Mol. Pharmacol.* **50**, 285-292
19. Sjodin, P., Holmberg, S. K., Akerberg, H., Berglund, M. M., Mohell, N., and Larhammar, D. (2006) Re-evaluation of receptor-ligand interactions of the human neuropeptide Y receptor Y1: a site-directed mutagenesis study. *Biochem. J.* **393**, 161-169

20. Merten, N., Lindner, D., Rabe, N., Rompler, H., Morl, K., Schoneberg, T., and Beck-Sickinger, A. G. (2007) Receptor subtype-specific docking of Asp6.59 with C-terminal arginine residues in Y receptor ligands. *J. Biol. Chem.* **282**, 7543-7551
21. Rathmann, D., Lindner, D., DeLuca, S. H., Kaufmann, K. W., Meiler, J., and Beck-Sickinger, A. G. (2012) Ligand-mimicking receptor variant discloses binding and activation mode of prolactin-releasing peptide. *J. Biol. Chem.* **287**, 32181-32194
22. Ballesteros, J. A., and Weinstein, H. (1995) Integrated methods for the construction of three-dimensional models and computational probing of structure-function relations in G protein-coupled receptors. *Methods Neurosci.* **25**, 366-428
23. Rathmann, D., Pedragosa-Badia, X., and Beck-Sickinger, A. G. (2013) In vitro modification of substituted cysteines as tool to study receptor functionality and structure-activity relationships. *Anal. Biochem.* **439**, 173-183
24. Leaver-Fay, A., Tyka, M., Lewis, S. M., Lange, O. F., Thompson, J., Jacak, R., Kaufman, K., Renfrew, P. D., Smith, C. A., Sheffler, W., Davis, I. W., Cooper, S., Treuille, A., Mandell, D. J., Richter, F., Ban, Y. E., Fleishman, S. J., Corn, J. E., Kim, D. E., Lyskov, S., Berrondo, M., Mentzer, S., Popovic, Z., Havranek, J. J., Karanicolas, J., Das, R., Meiler, J., Kortemme, T., Gray, J. J., Kuhlman, B., Baker, D., and Bradley, P. (2011) ROSETTA3: an object-oriented software suite for the simulation and design of macromolecules. *Methods. Enzymol.* **487**, 545-574
25. Okada, T., Sugihara, M., Bondar, A. N., Elstner, M., Entel, P., and Buss, V. (2004) The retinal conformation and its environment in rhodopsin in light of a new 2.2 Å crystal structure. *J. Mol. Biol.* **342**, 571-583
26. Cherezov, V., Rosenbaum, D. M., Hanson, M. A., Rasmussen, S. G., Thian, F. S., Kobilka, T. S., Choi, H. J., Kuhn, P., Weis, W. I., Kobilka, B. K., and Stevens, R. C. (2007) High-resolution crystal structure of an engineered human beta2-adrenergic G protein-coupled receptor. *Science* **318**, 1258-1265
27. Warne, T., Serrano-Vega, M. J., Baker, J. G., Moukhametzianov, R., Edwards, P. C., Henderson, R., Leslie, A. G., Tate, C. G., and Schertler, G. F. (2008) Structure of a beta1-adrenergic G-protein-coupled receptor. *Nature* **454**, 486-491
28. Jaakola, V. P., Griffith, M. T., Hanson, M. A., Cherezov, V., Chien, E. Y., Lane, J. R., Ijzerman, A. P., and Stevens, R. C. (2008) The 2.6 angstrom crystal structure of a human A2A adenosine receptor bound to an antagonist. *Science* **322**, 1211-1217
29. Wu, B., Chien, E. Y., Mol, C. D., Fenalti, G., Liu, W., Katritch, V., Abagyan, R., Brooun, A., Wells, P., Bi, F. C., Hamel, D. J., Kuhn, P., Handel, T. M., Cherezov, V., and Stevens, R. C. (2010) Structures of the CXCR4 chemokine GPCR with small-molecule and cyclic peptide antagonists. *Science* **330**, 1066-1071
30. Chien, E. Y., Liu, W., Zhao, Q., Katritch, V., Han, G. W., Hanson, M. A., Shi, L., Newman, A. H., Javitch, J. A., Cherezov, V., and Stevens, R. C. (2010) Structure of the human dopamine D3 receptor in complex with a D2/D3 selective antagonist. *Science* **330**, 1091-1095
31. Shimamura, T., Shiroishi, M., Weyand, S., Tsujimoto, H., Winter, G., Katritch, V., Abagyan, R., Cherezov, V., Liu, W., Han, G. W., Kobayashi, T., Stevens, R. C., and Iwata, S. (2011) Structure of the human histamine H1 receptor complex with doxepin. *Nature* **475**, 65-70
32. Haga, K., Kruse, A. C., Asada, H., Yurugi-Kobayashi, T., Shiroishi, M., Zhang, C., Weis, W. I., Okada, T., Kobilka, B. K., Haga, T., and Kobayashi, T. (2012) Structure of the human M2 muscarinic acetylcholine receptor bound to an antagonist. *Nature* **482**, 547-551
33. Hanson, M. A., Roth, C. B., Jo, E., Griffith, M. T., Scott, F. L., Reinhart, G., Desale, H., Clemons, B., Cahalan, S. M., Schuerer, S. C., Sanna, M. G., Han, G. W., Kuhn, P., Rosen, H., and Stevens, R. C. (2012) Crystal structure of a lipid G protein-coupled receptor. *Science* **335**, 851-855
34. Kruse, A. C., Hu, J., Pan, A. C., Arlow, D. H., Rosenbaum, D. M., Rosemond, E., Green, H. F., Liu, T., Chae, P. S., Dror, R. O., Shaw, D. E., Weis, W. I., Wess, J., and Kobilka, B. K. (2012) Structure and dynamics of the M3 muscarinic acetylcholine receptor. *Nature* **482**, 552-556
35. Wu, H., Wacker, D., Mileni, M., Katritch, V., Han, G. W., Vardy, E., Liu, W., Thompson, A. A., Huang, X. P., Carroll, F. I., Mascarella, S. W., Westkaemper, R. B., Mosier, P. D., Roth,

- B. L., Cherezov, V., and Stevens, R. C. (2012) Structure of the human kappa-opioid receptor in complex with JD1c. *Nature* **485**, 327-332
36. Manglik, A., Kruse, A. C., Kobilka, T. S., Thian, F. S., Mathiesen, J. M., Sunahara, R. K., Pardo, L., Weis, W. I., Kobilka, B. K., and Granier, S. (2012) Crystal structure of the micro-opioid receptor bound to a morphinan antagonist. *Nature* **485**, 321-326
37. Thompson, A. A., Liu, W., Chun, E., Katritch, V., Wu, H., Vardy, E., Huang, X. P., Trapella, C., Guerrini, R., Calo, G., Roth, B. L., Cherezov, V., and Stevens, R. C. (2012) Structure of the nociceptin/orphanin FQ receptor in complex with a peptide mimetic. *Nature* **485**, 395-399
38. Granier, S., Manglik, A., Kruse, A. C., Kobilka, T. S., Thian, F. S., Weis, W. I., and Kobilka, B. K. (2012) Structure of the delta-opioid receptor bound to naltrindole. *Nature* **485**, 400-404
39. Konagurthu, A. S., Whisstock, J. C., Stuckey, P. J., and Lesk, A. M. (2006) MUSTANG: a multiple structural alignment algorithm. *Proteins* **64**, 559-574
40. Thompson, J. D., Gibson, T. J., and Higgins, D. G. (2002) Multiple sequence alignment using ClustalW and ClustalX. in *Curr. Protoc. Bioinformatics* (Baxevanis, A. D. ed.), 2008/09/17 Ed. pp Unit 2 3
41. Canutescu, A. A., and Dunbrack, R. L., Jr. (2003) Cyclic coordinate descent: A robotics algorithm for protein loop closure. *Protein Sci.* **12**, 963-972
42. Yarov-Yarovoy, V., Schonbrun, J., and Baker, D. (2006) Multipass membrane protein structure prediction using Rosetta. *Proteins* **62**, 1010-1025
43. Alexander, N., Woetzel, N., and Meiler, J. (2011) Bcl::Cluster: A method for clustering biological molecules coupled with visualization in the Pymol Molecular Graphics System 1st IEEE International Conference on Computational Advances in Bio and Medical Sciences (ICCABS), Orlando, FL, February 3-5 2011
44. Lerch, M., Gafner, V., Bader, R., Christen, B., Folkers, G., and Zerbe, O. (2002) Bovine pancreatic polypeptide (bPP) undergoes significant changes in conformation and dynamics upon binding to DPC micelles. *J. Mol. Biol.* **322**, 1117-1133
45. Gehlert, D. R., Schober, D. A., Gackenhaimer, S. L., Beavers, L., Gadski, R., Lundell, I., and Larhammar, D. (1997) [125I]Leu31, Pro34-PYY is a high affinity radioligand for rat PP1/Y4 and Y1 receptors: evidence for heterogeneity in pancreatic polypeptide receptors. *Peptides* **18**, 397-401
46. Walker, M. W., Smith, K. E., Bard, J., Vaysse, P. J., Gerald, C., Daouti, S., Weinshank, R. L., and Branchek, T. A. (1997) A structure-activity analysis of the cloned rat and human Y4 receptors for pancreatic polypeptide. *Peptides* **18**, 609-612
47. Simons, K. T., Kooperberg, C., Huang, E., and Baker, D. (1997) Assembly of protein tertiary structures from fragments with similar local sequences using simulated annealing and Bayesian scoring functions. *J. Mol. Biol.* **268**, 209-225
48. Lindner, D., Stichel, J., and Beck-Sickinger, A. G. (2008) Molecular recognition of the NPY hormone family by their receptors. *Nutrition* **24**, 907-917
49. Dunbrack, R. L., Jr., and Karplus, M. (1993) Backbone-dependent rotamer library for proteins. Application to side-chain prediction. *J. Mol. Biol.* **230**, 543-574
50. Bradley, P., Misura, K. M., and Baker, D. (2005) Toward high-resolution de novo structure prediction for small proteins. *Science* **309**, 1868-1871
51. Misura, K. M., and Baker, D. (2005) Progress and challenges in high-resolution refinement of protein structure models. *Proteins* **59**, 15-29
52. Eckard, C. P., Cabrele, C., Wieland, H. A., and Beck-Sickinger, A. G. (2001) Characterisation of neuropeptide Y receptor subtypes by synthetic NPY analogues and by anti-receptor antibodies. *Molecules* **6**, 448-467
53. Klco, J. M., Nikiforovich, G. V., and Baranski, T. J. (2006) Genetic analysis of the first and third extracellular loops of the C5a receptor reveals an essential WXFG motif in the first loop. *J. Biol. Chem.* **281**, 12010-12019
54. Kanno, T., Kanatani, A., Keen, S. L., Arai-Otsuki, S., Haga, Y., Iwama, T., Ishihara, A., Sakuraba, A., Iwaasa, H., Hirose, M., Morishima, H., Fukami, T., and Ihara, M. (2001) Different binding sites for the neuropeptide Y Y1 antagonists 1229U91 and J-104870 on human Y1 receptors. *Peptides* **22**, 405-413

55. Tautermann, C. S., and Pautsch, A. (2011) The Implication of the First Agonist Bound Activated GPCR X-ray Structure on GPCR in Silico Modeling. *Acs Medicinal Chemistry Letters* **2**, 414-418
56. Beck-Sickinger, A. G., Wieland, H. A., Wittneben, H., Willim, K. D., Rudolf, K., and Jung, G. (1994) Complete L-alanine scan of neuropeptide Y reveals ligands binding to Y1 and Y2 receptors with distinguished conformations. *Eur. J. Biochem.* **225**, 947-958
57. Raman, B., Guarnaccia, C., Nadassy, K., Zakhariev, S., Pintar, A., Zanuttin, F., Frigyes, D., Acatrinei, C., Vindigni, A., Pongor, G., and Pongor, S. (2001) N(omega)-arginine dimethylation modulates the interaction between a Gly/Arg-rich peptide from human nucleolin and nucleic acids. *Nucleic Acids Res.* **29**, 3377-3384
58. Sylte, I., Andrianjara, C. R., Calvet, A., Pascal, Y., and Dahl, S. G. (1999) Molecular dynamics of NPY Y1 receptor activation. *Bioorg. Med. Chem.* **7**, 2737-2748

Acknowledgements- We thank Regina Reppich-Sacher, Kristin Löbner and Janet Schwesinger for technical support. We also thank Daniel Rathmann and René Meier for research discussions, Stephanie DeLuca for her assistance in developing the peptide docking protocols and Eric Dawson for developing preliminary comparative models.

FOOTNOTES

*This work was supported in whole or in part by German Research Foundation Grants (DFG, SFB 610/3-A1 and BE 1264-11) (to A.B.-S), NIH Grants (R01 GM080403, R01 MH090192, R01 GM099842), NSF Grant (Career 0742762) (to J.M) and NIH Grant (R01 DK097376) (to J.M and A. B.-S.). This work was further supported through a pilot & feasibility study from the Vanderbilt Diabetes Research and Training Center (DRTC) and through a NSF award to explore international collaboration (OISE 1157751)

[†]This article contains supplementary material.

¹Present address:

Diana Lindner. Dept. of general and interventional cardiology, University Heart Center Hamburg, Maritinstr. 52, 20246 Hamburg, Germany.

Kristian W.Kaufmann. Dept. of Pharmacology, Vanderbilt University, 2220 Pierce Avenue, TN 37212, USA.

²To whom the correspondence should be addressed:

Annette G. Beck-Sickinger, Institute of Biochemistry, Faculty of Biosciences, Pharmacy and Psychology, Universität Leipzig, Brüderstraße 34, 04103 Leipzig, Germany. Phone: +493419736900. Fax: +49493419736909. E-mail: beck-sickinger@uni-leipzig.de

Jens Meiler, Center for Structural Biology, Vanderbilt University, 5144B Biosci/MRBIII, 465 21st Avenue South, Nashville, TN 37232-8725, USA. Phone: +16159365662. Fax: +16159362211. E-mail: jens@meilerlab.org

³The abbreviations used are: hY₄R, human Y₄R; hPP, human pancreatic polypeptide; GPCR, G protein-coupled receptors; TM, transmembrane helix; ECL, extracellular loop; NPFFR, neuropeptide FF receptor; NPY, neuropeptide Y; PYY, peptide YY; PrRPR, prolactin-releasing peptide receptor; SPPS, solid phase peptide synthesis; PDB, protein data bank; MSA, multiple sequence alignment; MCM, Monte Carlo Metropolis; CCD, loop closure algorithms; SDMA, symmetrically dimethylated Arg; ADMA, asymmetrically dimethylated Arg; C5aR, complement factor 5a receptor; CXCR4, CXC chemokine receptor type 4; NTSR1, neurotensin receptor 1; OxR, orexin receptor.

^aEC₅₀ and pEC₅₀ values were determined from the mean S.E. of n independent experiments, each performed in duplicate.

^bThe ratio was calculated using the global fitting function for EC₅₀ shift determination of Prism 5.03.

^cThe Emax was determined at the highest peptide concentration.

^dNT represents not tested.

^eND represents non-determined because the curve could not reach the plateau.

FIGURE LEGENDS

FIGURE 1. hY₄R comparative model and PP docking workflow. An ensemble of hY₄R comparative models was constructed through several rounds of loop building and energy minimization followed by selection of the best models. Alongside the flowchart are representative models to illustrate the evolution of the comparative model. hPP was docked through the placement of the PP helix, *de novo* addition of the C-terminal residues, and finally the addition of the ECLs of hY₄R. Those steps were guided by experimentally derived restraints and followed by selection of the top models.

FIGURE 2. A. Alignment of the NPY receptor sequences. Highlighted residues are conserved or partially conserved amino acids within the receptor subfamily. B. Snake plot showing the sequence of hY₄R. Residues in light grey show residues investigated with no influence in activity. Residues in dark grey show an influence in receptor activity. Residues in black have an interaction partner on the peptide side. C. Alignment of the NPY ligand sequences.

FIGURE 3. Concentration response curves of hY₄R receptor mutants and hPP analogs determined with an IP accumulation assay. A. Functional characterization of Y₄R mutant Tyr^{2.64}Ala with the modified ligands [Ala²⁷]hPP and [Cha²⁷]hPP to study the influence between Tyr^{2.64} of hY₄R and Tyr²⁷ of hPP. B. Functional investigation of hY₄R mutant Asp^{2.68}Ala.

FIGURE 4. Cell surface expression of Y₄R and Y₄R mutants, Tyr^{2.64}Ala, Tyr^{2.64}Leu, Asp^{2.68}Ala, Asp^{2.68}Glu, Asp^{2.68}Asn, Tyr^{5.38}Ala, Asn^{6.55}Ala, Asn^{7.32}A, Asn^{7.32}Asp, Asn^{7.32}Arg, Phe^{7.35}Ala and Phe^{7.35}Ile. HEK-293 cells were transiently transfected with hY₄R constructs C-terminally fused to eYFP. The nucleus was developed using Hoechst 33342. Scale bar represents 10µm.

FIGURE 5. Concentration response curves obtained with an IP accumulation assay using increasing concentration of the ligands. A. Functional characterization of hY₄R mutants Asn^{6.55}Ala. B. Investigation of the relationship between position 33 of hPP and the amino acids Asn^{7.32} of hY₄R using the ligands hPP, [ADMA³³]hPP and [Lys³³]hPP.

FIGURE 6. Concentration response curves were determined with an IP accumulation assay with increasing concentration of the analogs. Functional investigations are shown for position 36 of hPP and Phe^{7.35} of hY₄R. COS-7 cells were transiently co-transfected with hY₄R constructs and the chimeric G protein Gα_{Δ6qi4myr}.

FIGURE 7. Characterization of the binding pocket of PP docked in the hY₄R comparative model. A. Side view of PP (purple) docked to hY₄R (cyan). Residues found to be important in the activation of hY₄R by hPP are labeled. Predicted interactions are indicated by dotted red lines (salt bridge between Asp^{6.59} and Arg³⁵ and hydrogen bond between Arg³³ and Asn^{7.32}). B. Top-down view of the same docked model. C. Two docked models show the variability in ECL1. The model shown in gray has a significantly longer ECL1 than that shown in cyan. Trp^{2.70}, which was experimentally shown to be important in hY₄R activation by PP is shown to be in different proximity to PP depending on the size of ECL1. D. Side view of the same docked model shown in A and B. Residues experimentally shown to be inactive in the binding of hPP to hY₄R are indicated in black. The disulfide bond in ECL2 is also shown in yellow. a=His^{7.39}, b=Gln^{3.32}, c=Phe^{6.54}, d=His^{6.62}, e=Tyr^{5.38}, f=His^{5.34}, g=Trp^{5.29}, h=Phe^{4.80}, i=Glu^{4.67}, j=Glu^{4.79}, k=Lys^{4.72}, l=Asp^{4.83}

FIGURE 8. hY₄R and PP residues within an 8 angstrom distance (based on C-β atoms) represent possible binding interactions. Neighboring residue pairs were collected across the 9 final PP- hY₄R docked models and presented as a heatmap indicating the most represented neighbors. hY₄R residues are listed on the x-axis with their secondary structure indicated (orange = TM, blue = ECL). PP residues are listed on the y-axis with similar secondary structure indications. Numbers represent the number of models (out of 9) from which these residue pairs were within 8 angstroms. TM = Transmembrane; ICL = Intracellular Loop; ECL = Extracellular Loop

TABLE 1. Experimental restraints used to guide docking of PP with hY₄R

hY ₄ R residue	PP residue	Low-resolution restraint	High-resolution restraint	Proposed interaction	Steps imposed	Experimental evidence
Tyr ^{2,64}	Tyr ²⁷	C-β atoms within 8 Å	None	Unknown	hPP helix placement	Table 2 (Tyr ^{2,64} and Tyr ²⁷ single mutants)
Asp ^{6,59}	Arg ³⁵	C-β atoms within 8 Å	Asp ^{6,59} O-δ and Arg ³³ NH within 4 Å	Salt bridge	hPP C-term folding (low resolution), hY4R loop building (low resolution), final relaxation (high resolution)	Reference 20
Asn ^{7,32}	Arg ³³	C-β atoms within 8 Å	Asn ^{7,32} O-δ and Arg ³³ NH within 4 Å	Hydrogen bond	hPP C-term folding (low resolution), hY4R loop building (low resolution), final relaxation (high resolution)	Table 5, Figure 5B (Asp ^{6,59} and Arg ³⁵ single mutants)
Phe ^{7,35}	Arg ³³	C-β atoms within 8 Å	None	Pi-cation stacking	hPP C-term folding (low resolution), hY4R loop building (low resolution), final relaxation (high resolution)	Reference 50, Table 6 (Phe ^{7,35} and Arg ³³ single mutants)
Phe ^{7,35}	Tyr ³⁶	None	Phe ^{7,35} CZ and Tyr ³⁶ CZ within 4 Å	Unknown	Final relaxation (high resolution)	Table 6, Figure 6 (Phe ^{7,35} and Tyr ³⁶ single mutants)

TABLE 2. Signal transduction of hY₄ receptor mutants, mutated residues located on TM2. The IP accumulation assays were performed using increasing concentrations of hPP, [Ala²⁷]hPP, [Leu²⁷]hPP, [Cha²⁷]hPP and [Phe²⁷]hPP: The incubation time lasted for 1h. EC₅₀ values from dose-response curves were determined. *n* represents the number of independent experiments, each performed in duplicate.

Peptides	Wild type			Tyr ^{2,64} Ala			Tyr ^{2,64} Leu			Tyr ^{2,64} Phe		
	EC ₅₀ (nM) ^a (pEC ₅₀ ± SEM)	EC ₅₀ ratio ^b (mutant/ wild type)	n	EC ₅₀ (nM) ^a (pEC ₅₀ ± SEM)	EC ₅₀ ratio ^b (mutant/ wild type)	n	EC ₅₀ (nM) ^a (pEC ₅₀ ± SEM)	EC ₅₀ ratio ^b (mutant/ wild type)	n	EC ₅₀ (nM) ^a (pEC ₅₀ ± SEM)	EC ₅₀ ratio ^b (mutant/ wild type)	n
hPP	1.44 (8.84 ± 0.04)	1	39	93.20 (7.03 ± 0.09)	65	7	1.30 (8.89 ± 0.11)	0.9	4	6.13 (8.21 ± 0.09)	4	5
[Ala ²⁷]hPP	11.78 (7.93 ± 0.08)	8	4	579.90 (6.24 ± 0.15)	424	4	205.20 (6.69 ± 0.09)	138	3	NT ^d	-	-
[Leu ²⁷]hPP	1.19 (8.92 ± 0.17)	0.85	4	90.63 (7.04 ± 0.14)	63	4	32.20 (7.49 ± 0.09)	21	3	NT ^d	-	-
[Cha ²⁷]hPP	2.81 (8.55 ± 0.09)	2	7	22.34 (7.65 ± 0.17)	14	4	33.45 (7.48 ± 0.14)	23	2	NT ^d	-	-
[Phe ²⁷]hPP	0.852 (9.07 ± 0.12)	0.6	4	NT ^d	-	-	NT ^d	-	-	11.26 (7.95 ± 0.11)	9	4

TABLE 3. Signal transduction of hY₄ receptor mutants, mutated residues located on the ECL1 and TM3. The IP accumulation assays were performed using increasing concentrations of hPP for 1h. EC₅₀ values from dose-response curves were determined. *n* represents the number of independent experiments, each performed in duplicate.

Y ₄ R mutants	hPP			n
	EC ₅₀ (nM) ^a (pEC ₅₀ ± SEM)	EC ₅₀ ratio ^b (mutant/ wild type)	E _{max} ± SEM ^c	
Wild type	1.44 (8.84 ± 0.04)	1	100	39
Asp ^{2.68} Ala	135 (6.87 ± 0.24)	94	39 ± 2	3
Asp ^{2.68} Glu	13.66 (7.87 ± 0.18)	9	93 ± 4	2
Asp ^{2.68} Asn	22.88 (7.64 ± 0.13)	16	87 ± 3	2
Trp ^{2.70} Ala	157.7 (6.80 ± 0.36)	107	95 ± 9.5	6
Trp ^{2.70} Tyr	3.06 (8.52 ± 0.45)	2	108 ± 7	2
Gln ^{3.32} Ala	1.25 (8.90 ± 0.22)	0.87	95 ± 4	3

TABLE 4. Signal transduction results of ECL2 and TM5 mutants of the hY₄ receptor. The IP accumulation assays were performed using increasing concentrations of hPP for 1h. EC₅₀ values from dose-response curves were determined. *n* represents the number of independent experiments, each performed in duplicate.

Y ₄ R mutants	hPP			n
	EC ₅₀ (nM) ^a (pEC ₅₀ ± SEM)	EC ₅₀ ratio ^b (mutant/ wild type)	E _{max} ± SEM ^c	
Wild type	1.44 (8.84 ± 0.04)	1	100	39
Glu ^{4.67} Ala	2.74 (8.56 ± 0.30)	2	88 ± 6	2
Lys ^{4.72} Ala	5.07 (8.30 ± 0.17)	4	105 ± 5	2
Glu ^{4.79} Ala	1.77 (8.75 ± 0.20)	1	114 ± 6	2
Phe ^{4.80} Ala	1.58 (8.8 ± 0.24)	1	100 ± 6	2
Asp ^{4.83} Ala	2.58 (8.59 ± 0.15)	2	88 ± 3	3
Trp ^{5.29} Ala	4.03 (8.40 ± 0.17)	3	96 ± 4	3
His ^{5.34} Ala	1.26 (8.89 ± 0.33)	0.9	86 ± 7	3
Tyr ^{5.38} Ala	1.36 (8.87±0.11)	0.9	44 ± 3	5
Tyr ^{5.38} Ser	4.19 (8.38± 0.18)	3	73 ± 3	5
Tyr ^{5.38} Phe	1.637 (8.79± 0.29)	1	109 ± 6	5
Phe ^{5.41} Ala	5.02 (8.30 ± 0.24)	4	92 ± 6	3

TABLE 5. Signal transduction of hY₄ receptor mutants, mutated residues located on the TM6, ECL3 and TM7. A. The IP accumulation assays were performed using increasing concentrations of hPP, [Lys³³]hPP, [ADMA³³]hPP or [SDMA³³]hPP. The incubation time lasted for 1h. EC₅₀ values from dose-response curves were determined, each performed in duplicate. *n* represents the number of independent experiments.

Y ₄ R mutants	hPP				[Lys ³³]hPP			[ADMA ³³]hPP			[SDMA ³³]hPP		
	EC ₅₀ (nM) ^a (pEC ₅₀ ± SEM)	EC ₅₀ ratio ^b (mutant/wild type)	E _{max} ± SEM ^c	n	EC ₅₀ (nM) ^a (pEC ₅₀ ± SEM)	EC ₅₀ ratio ^b (mutant/wild type)	n	EC ₅₀ (nM) ^a (pEC ₅₀ ± SEM)	EC ₅₀ ratio ^b (mutant/wild type)	n	EC ₅₀ (nM) ^a (pEC ₅₀ ± SEM)	EC ₅₀ ratio ^b (mutant/wild type)	n
Wild type	1.44 (8.84 ± 0.04)	1	100	39	1.68 (8.78 ± 0.07)	1	9	9.67 (8.02 ± 0.07)	7	9	9.13 (8.04 ± 0.08)	6	4
Phe ^{6,54} Ala	4.46 (8.35 ± 0.34)	4	73 ± 6	3	NT ^d	-	-	NT ^d	-	-	NT ^d	-	-
His ^{6,62} Ala	0.42 (9.37 ± 0.24)	0.33	98 ± 5	2	NT ^d	-	-	NT ^d	-	-	NT ^d	-	-
Asn ^{6,55} Ala	11.39 (7.94 ± 0.10)	8	79 ± 2	2	NT ^d	-	-	NT ^d	-	-	NT ^d	-	-
Asn ^{7,32} Ala	6.92 (8.16 ± 0.26)	5	84 ± 5	7	87.78 (7.06 ± 0.17)	60	3	1416 (5.85 ± 0.14)	979	4	2963 (5.53 ± 0.17)	1892	3
Asn ^{7,32} Arg	24.54 (7.61 ± 0.12)	18	107 ± 3	4	NT ^d	-	-	NT ^d	-	-	NT ^d	-	-
Asn ^{7,32} Asp	2.02 (8.69 ± 0.16)	1	97 ± 4	3	3.34 (8.48 ± 0.21)	2	3	4.24 (8.37 ± 0.23)	3	3	NT ^d	-	-

TABLE 6. Signal transduction of wild type, Phe^{7.35}Ala and Phe^{7.35}Ile receptors. The IP accumulation assays were performed using increasing concentrations of hPP as well as with hPP ligands with modifications on position Arg³³ or Tyr³⁶: [ADMA³³]hPP or [Lys³³]hPP, [Ala³⁶]hPP, [Ile³⁶]hPP, [Phe³⁶]hPP, [Cha³⁶]hPP or [Nle³⁶]hPP. The incubation time lasted for 1h. EC₅₀ values from concentration-response curves were determined. *n* represents the number of independent experiments, each performed in duplicate.

Peptides	Wild type				Phe ^{7.35} Ala				Phe ^{7.35} Ile			
	EC ₅₀ (nM) ^a (pEC ₅₀ ± SEM)	EC ₅₀ ratio ^b (mutant/ wild type)	E _{max} ± SEM ^c	n	EC ₅₀ (nM) ^a (pEC ₅₀ ± SEM)	EC ₅₀ ratio ^b (mutant/ wild type)	E _{max} ± SEM ^c	n	EC ₅₀ (nM) ^a (pEC ₅₀ ± SEM)	EC ₅₀ ratio ^b (mutant/ wild type)	E _{max} ± SEM ^c	n
hPP	1.44 (8.84 ± 0.04)	1	100	39	11.63 (7.93 ± 0.11)	8	99 ± 3	11	57.76 (7.24 ± 0.11)	41	58 ± 2	7
[ADMA ³³]hPP	9.67 (8.02 ± 0.07)	7	97 ± 2	9	160.5 (6.79 ± 0.15)	107	78 ± 4	2	>5000	ND	37 ± 3	3
[Lys ³³]hPP	1.68 (8.78 ± 0.07)	1	98 ± 2	9	640.4 (6.19 ± 0.14)	451	93 ± 4	3	1153 (5.95 ± 0.10)	762	48 ± 1	3
[Ala ³⁶]hPP	>2000	ND ^c	104 ± 11	3	NT ^d	-	-	-	NT ^d	-	-	-
[Ile ³⁶]hPP	191 (6.72 ± 0.15)	123	99 ± 4	3	ND	ND	-	3	NT ^d	-	-	-
[Phe ³⁶]hPP	2.07 (8.68 ± 0.23)	1	102 ± 4	4	25.29 (7.60 ± 0.43)	17	138 ± 15	3	NT ^d	-	-	-
[Cha ³⁶]hPP	0.76 (9.14 ± 0.18)	0.6	107 ± 4	3	211.2 (6.67 ± 0.09)	138	93 ± 3	3	NT ^d	-	-	-
[Nle ³⁶]hPP	14.40 (7.84 ± 0.16)	10	100 ± 4	5	1030 (5.99 ± 0.14)	679	81 ± 4	4	NT ^d	-	-	-

FIGURE 1

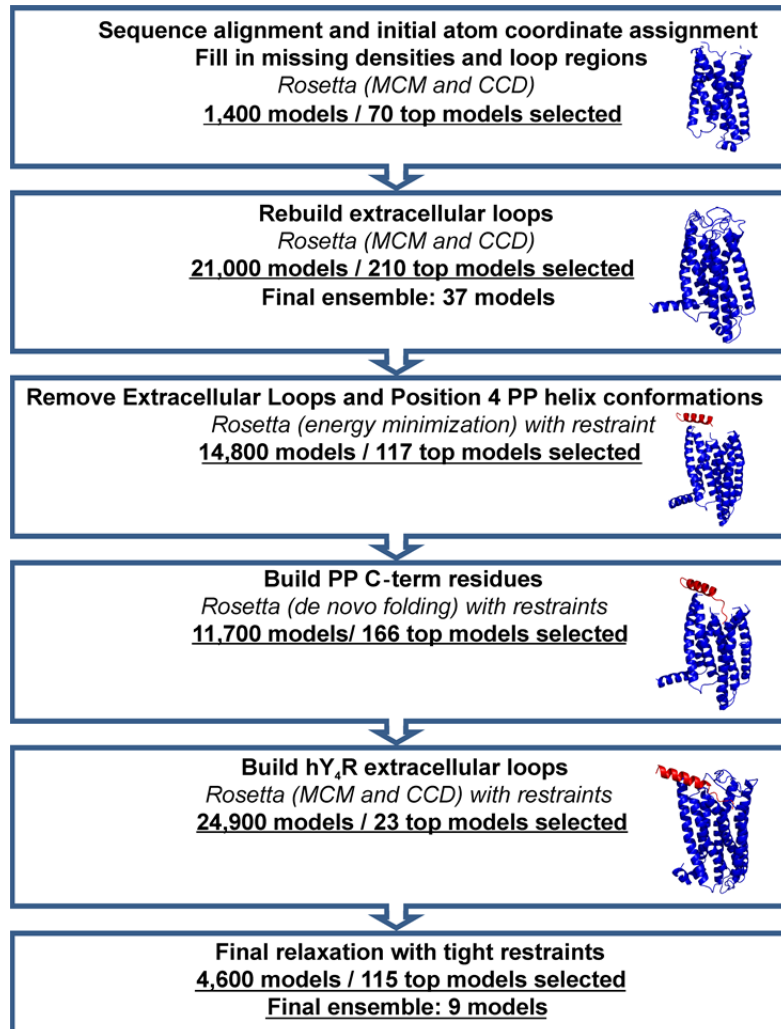


FIGURE 2

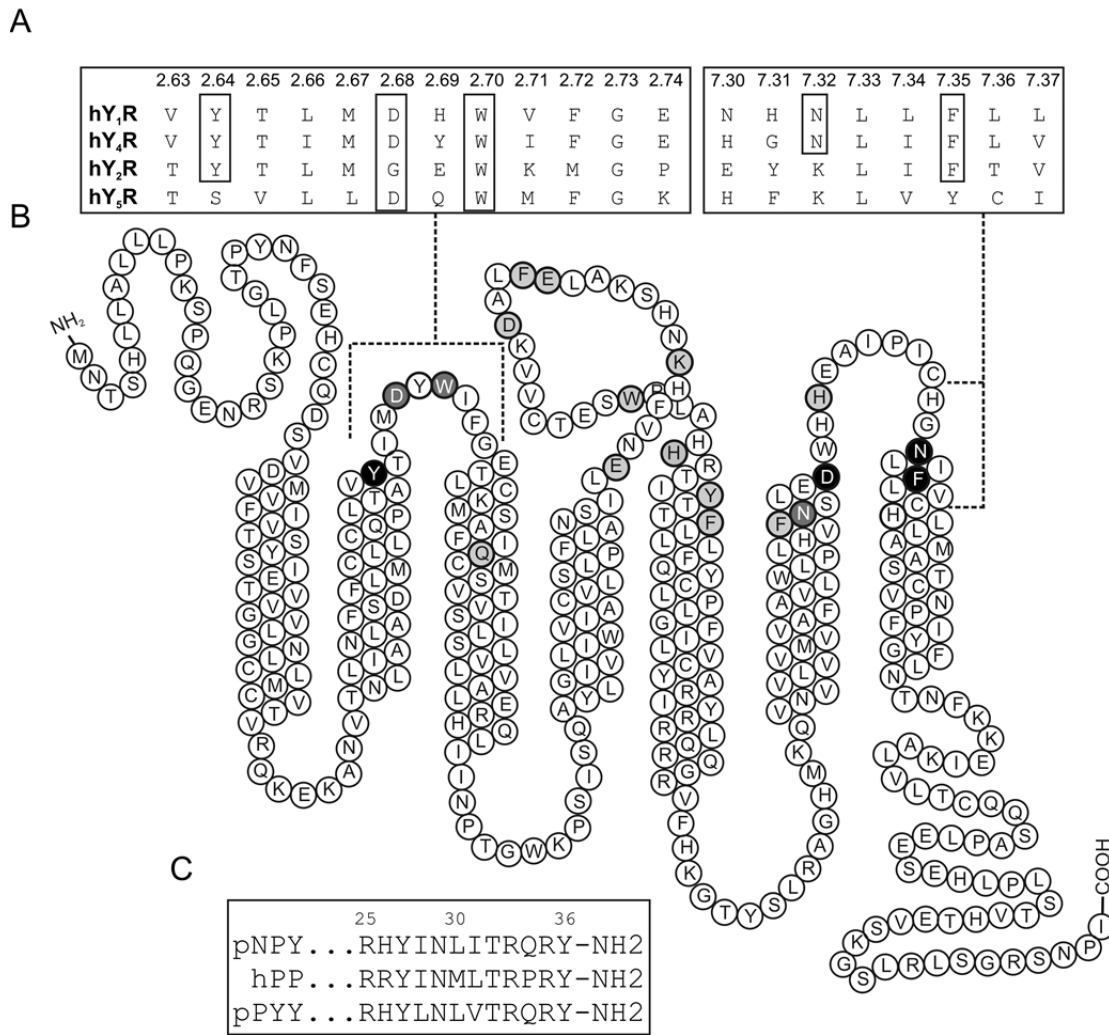


FIGURE 3

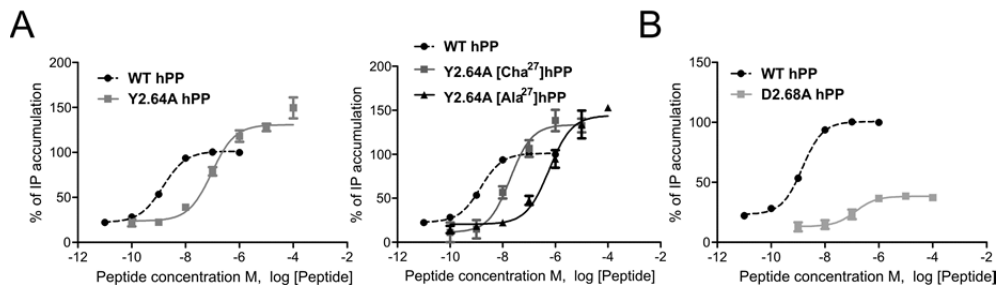


FIGURE 4

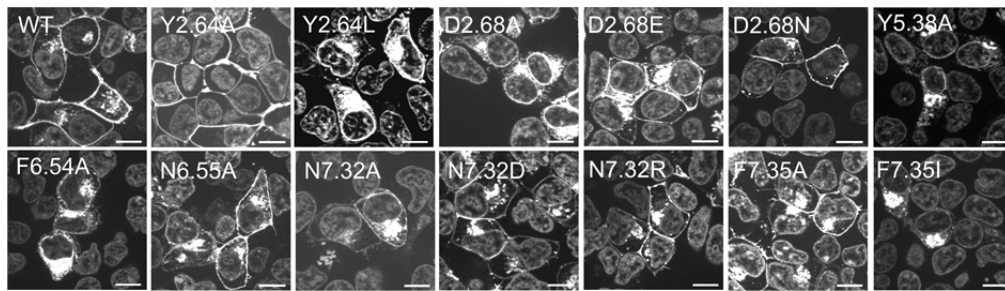


FIGURE 5

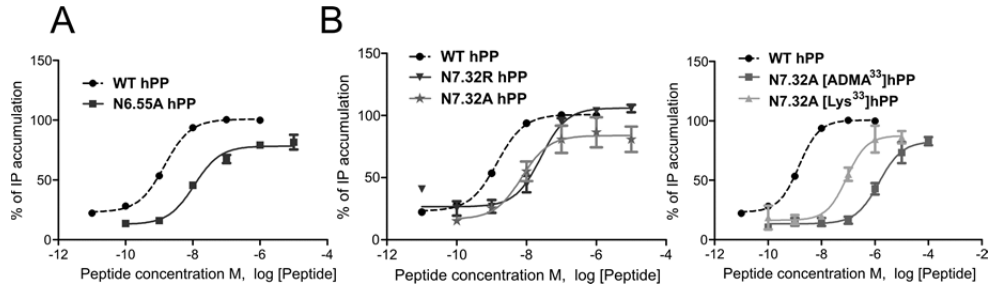


FIGURE 6

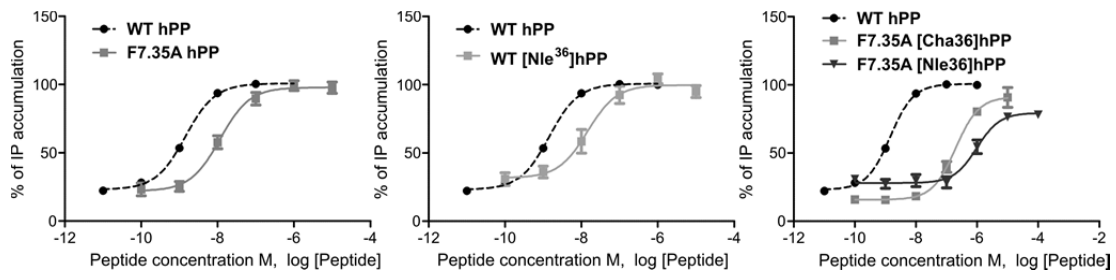


FIGURE 7

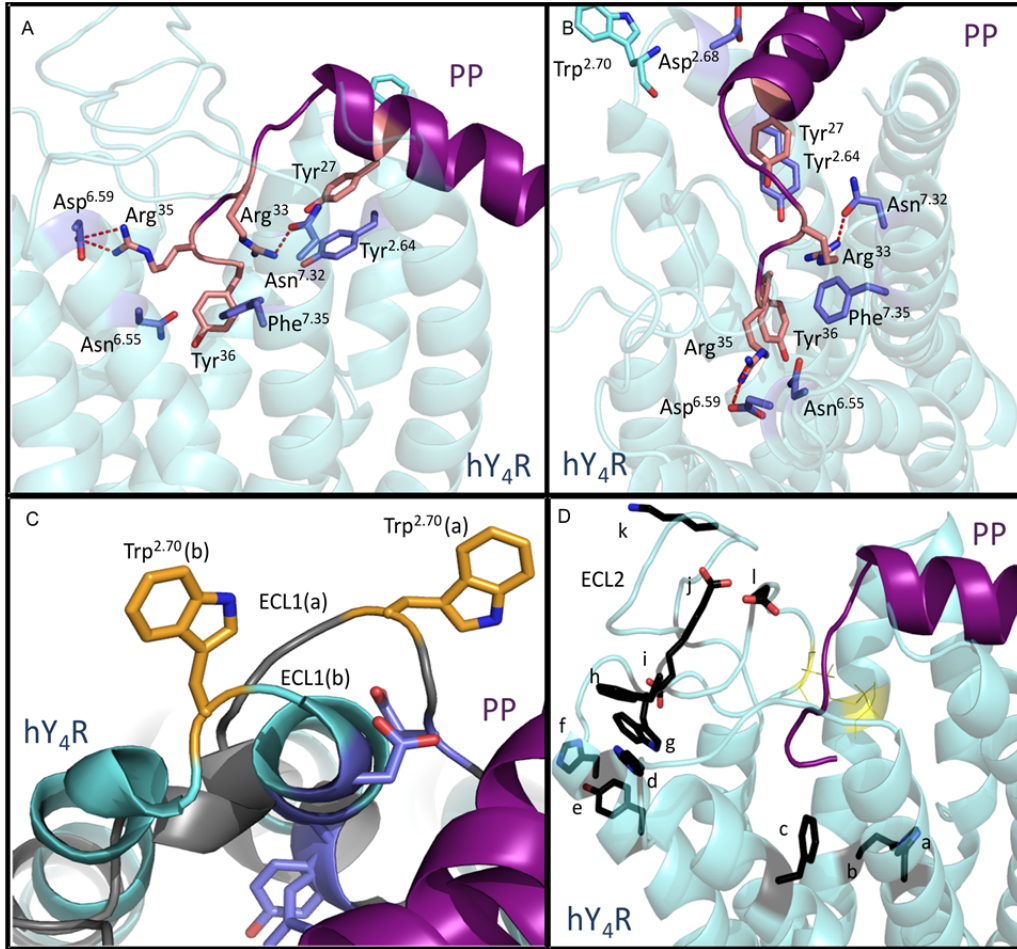


FIGURE 8

